Electronic Supplementary Material (ESI) for Physical Chemistry Chemical Physics.

Supporting information

Determining surface-specific Hubbard-U corrections and identifying key adsorbates on nickel and cobalt oxide catalyst surfaces

Shang Jiang[1] and Samir H. Mushrif[1]*
[1]*Department of Chemical and Materials Engineering, University of Alberta, 9211-116 Street Northwest, Edmonton, Alberta T6G 1H9, Canada*
Email: mushrif@ualberta.ca (SHM)

1. Benchmarking of computational parameters for NiO

Figure S1 shows the DFT+U optimized lattice parameter for NiO using different U values. The experimentally measured lattice parameter for NiO is ~4.176A and the difference is around 1% despite of the choice of the U values. The lattice parameter optimized for every U value is used for further calculation for each respective U value. Figure S2 shows the most stable magnetic ordering, row-by-row, which is more stable compared to bulk-like and layer-by-layer to NiO(100) structure. The computational core level binding energy for atoms is very sensitive to the local environment of catalyst surface. Hence, it is important to benchmark the thickness of the slab to ensure that the atoms at the central layers are capable of representing the bulk site, which will act as reference for core level binding energy shifts. Figure S3 shows the convergence test for slab thickness and a seven-layer model is chosen. Other computational parameters such as energy cut-off, the choice of K-point, and energy convergence criteria are also benchmarked to ensure that the calculated XPS shift is only related to the change in U value. Hence, NiO was modelled as a periodic seven-layer slab and a 10 Å vacuum thickness above the top layer was used to prevent the interaction between repeated periodic unit cells. The top five layers and the adsorbates were allowed to fully relax while the bottom two layers were fixed at the optimized bulk lattice parameters to reduce the computational cost without influencing the accuracy of simulations. The convergence criteria for total energy and interatomic forces were set to 10^{-6} eV and 0.01eV/A, respectively. All the calculations were performed with spin polarization as the antiferromagnetic ground state of NiO. The 3 × 4 × 1 Monkhorst–Pack grid was used to sample the Brillouin zone, and the tetrahedron method with Blöchl corrections was employed for all calculations. The representation of NiO model is shown in Figure S4.

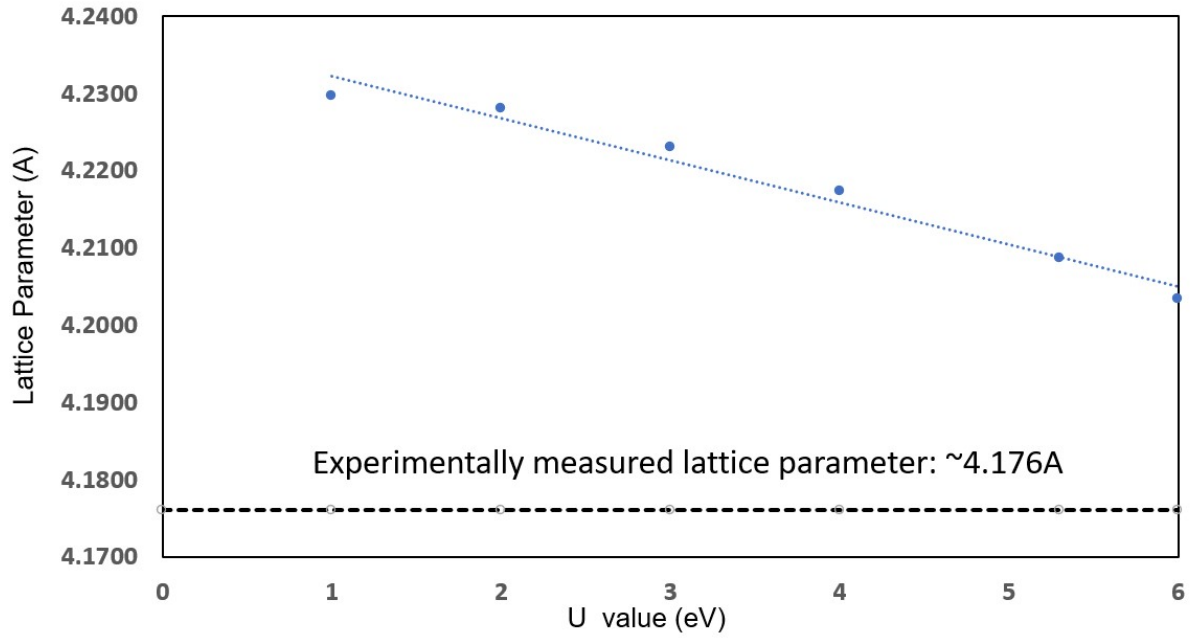

Figure S1. DFT+U optimized lattice parameter for NiO using different U values, in comparison with experimentally measured lattice parameter

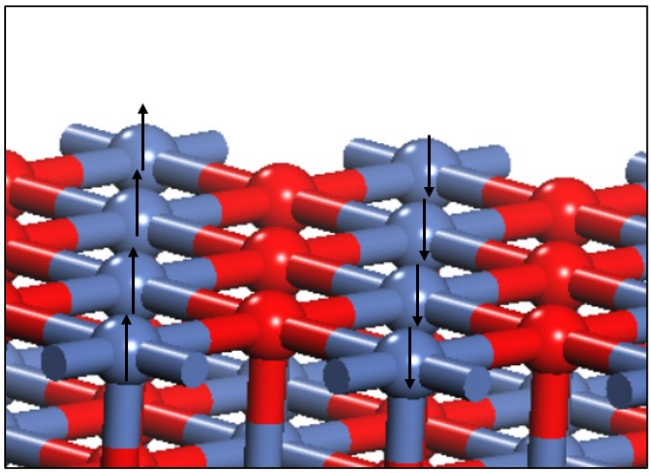

Figure S2. Magnetic arrangement for NiO (100), showing row-by-row magnetic spin ordering (where the alternating atoms of Ni in any particular row have same magnetic spins.) The upward and downward arrows represent the possitive and negative spin, respectively. Dark blue and red balls represent nickel (Ni) and oxygen (O) atoms, respectively.

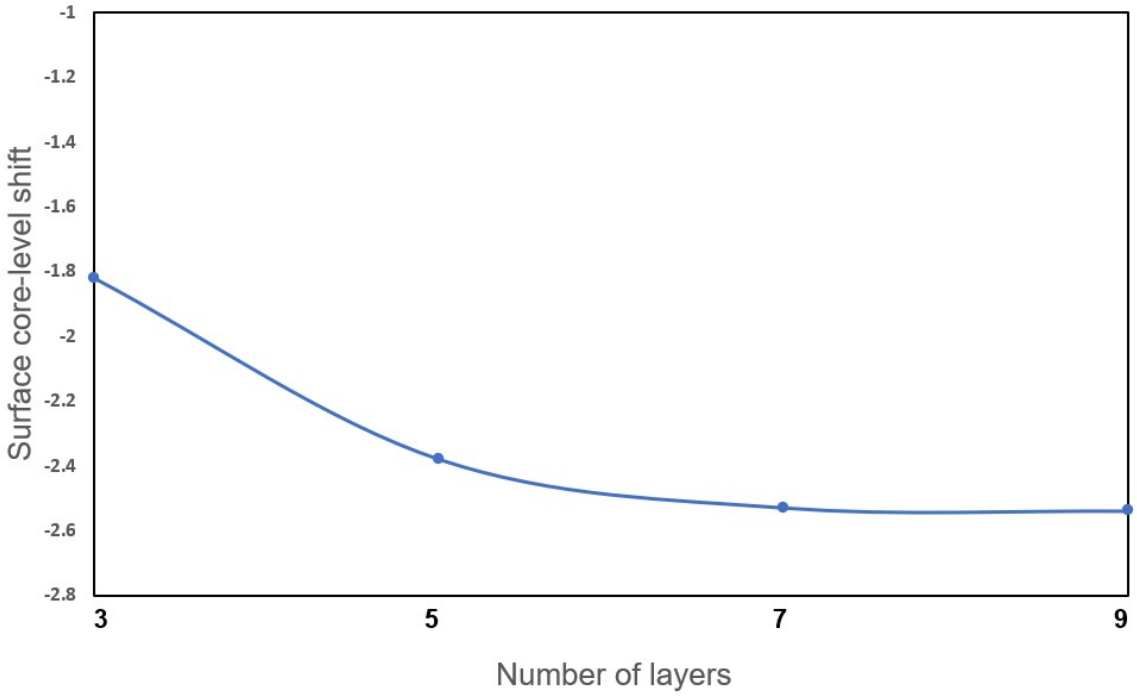

Figure S3. Convergence test showing the variation in calculated surface core level binding energy shifts for surface lattice oxygen, with increasing slab thickness (number of layers).

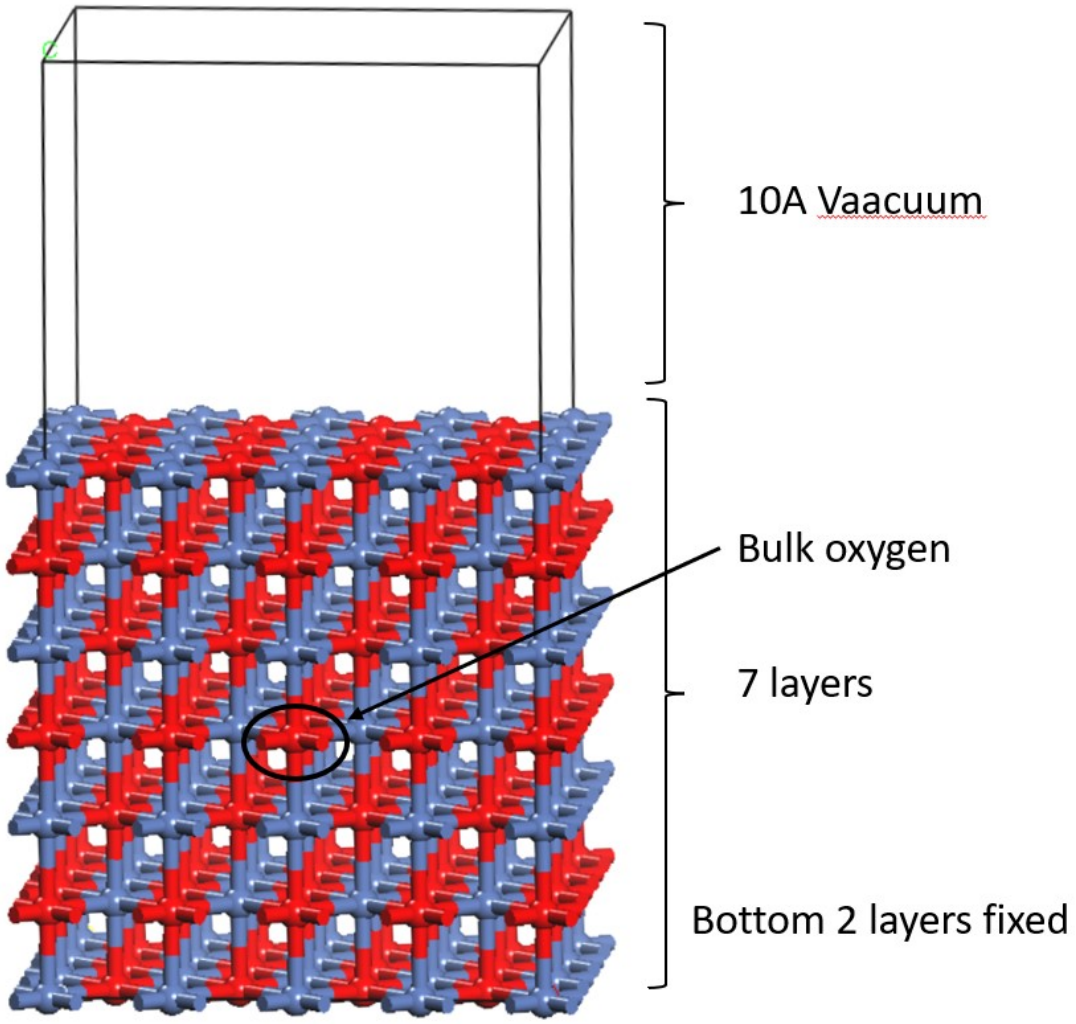

Figure S4. Representation of the system used to module NiO (100) surface, slab size, illustrating the number of layers and vacuum thickness. The oxygen atom in the central layers representing the bulk oxygen is highlighted. Dark blue and red balls represent nickel (Ni) and oxygen (O) atoms, respectively.

2. Benchmarking of computational parameters for Co_3O_4

Similar benchmarking procedures (as those of NiO) were performed on Co_3O_4 as well. Figure S5 shows the DFT calculated lattice parameter at various U values. Figure S6 shows the most stable magnetic arrangement. Figure S7 shows the convergence test to determine the thickness of the slab. Figure S8 shows the representation of Co_3O_4 model used. The terminal layer of Co_3O_4 (100) contains four cobalt atoms and eight oxygen atoms, and this termination is slightly more stable compared to the alternative, which only contains two cobalt atoms, according to our DFT calculations. In summary, Co_3O_4 was modelled as a periodic ten-layer slab and a 10 Å vacuum thickness above the top layer was used to prevent the interaction between repeated periodic unit cells. The top seven layers and the adsorbates were allowed to fully relax while the bottom three layers were fixed at the optimized bulk lattice parameters to reduce the computational cost without influencing the accuracy of simulations. The convergence criteria for total energy and interatomic forces were set to 10^{-6} eV per unit cell and 0.01eV/A, respectively. All the calculations were performed with spin polarization as the antiferromagnetic ground state of Co_3O_4. The $3 \times 4 \times 1$ Monkhorst–Pack grid was used to sample the Brillouin zone, and the tetrahedron method with Blöchl corrections was employed for all calculations.

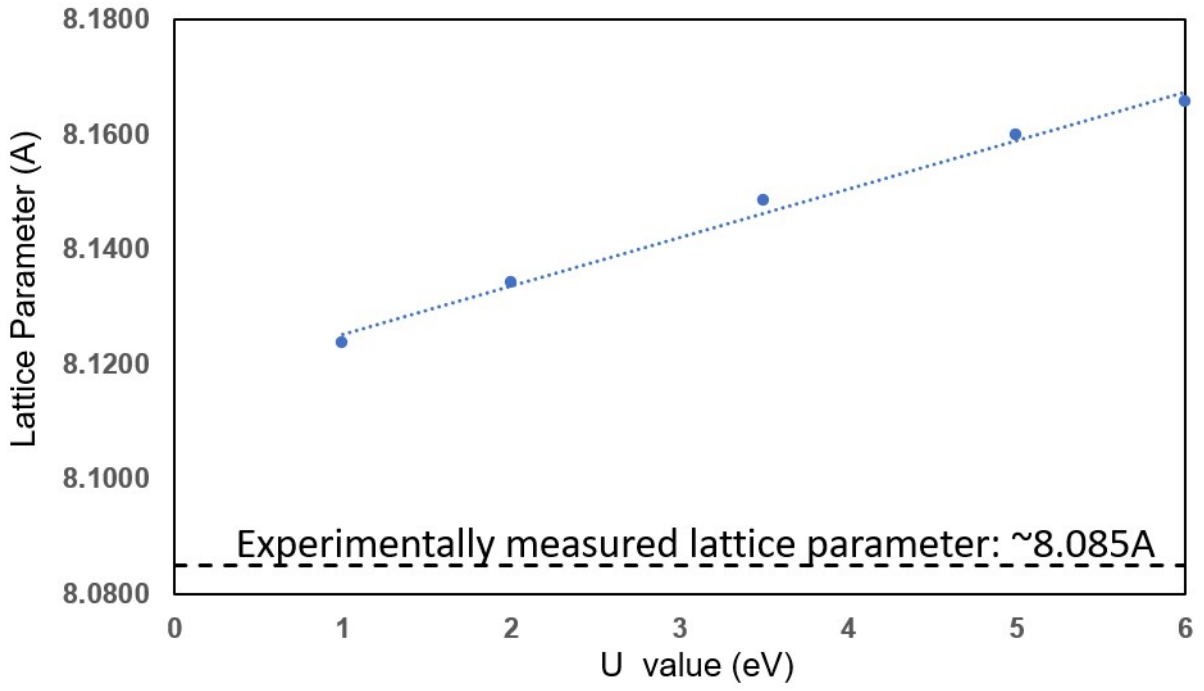

Figure S5. DFT+U optimized lattice parameter for Co_3O_4 using different U values in comparison with experimentally measured lattice parameter

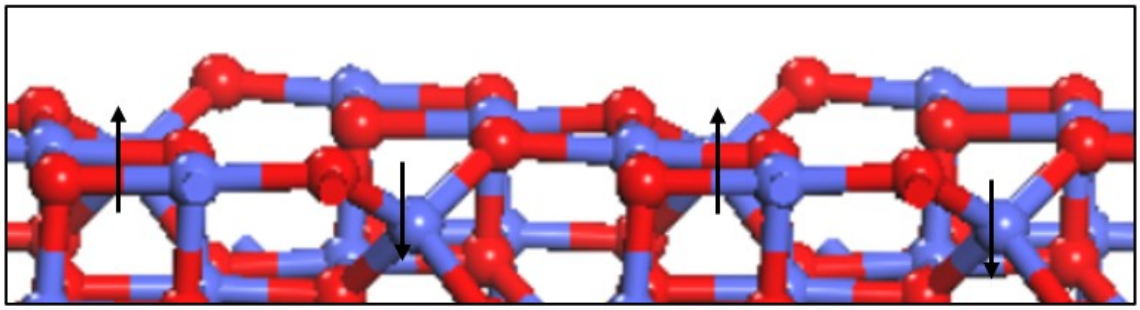

Figure S6. Magnetic arrangement for Co_3O_4 (100), showing row-by-row magnetic spin ordering (where the alternating atoms of Co^{2+} in any particular layer have alternative magnetic spins, and Co^{3+} have 0 magnetic moment) The upward and downward arrows represent the possitive and negative spin, respectively Light blue and red balls represent nickel (Co) and oxygen (O) atoms, respectively.

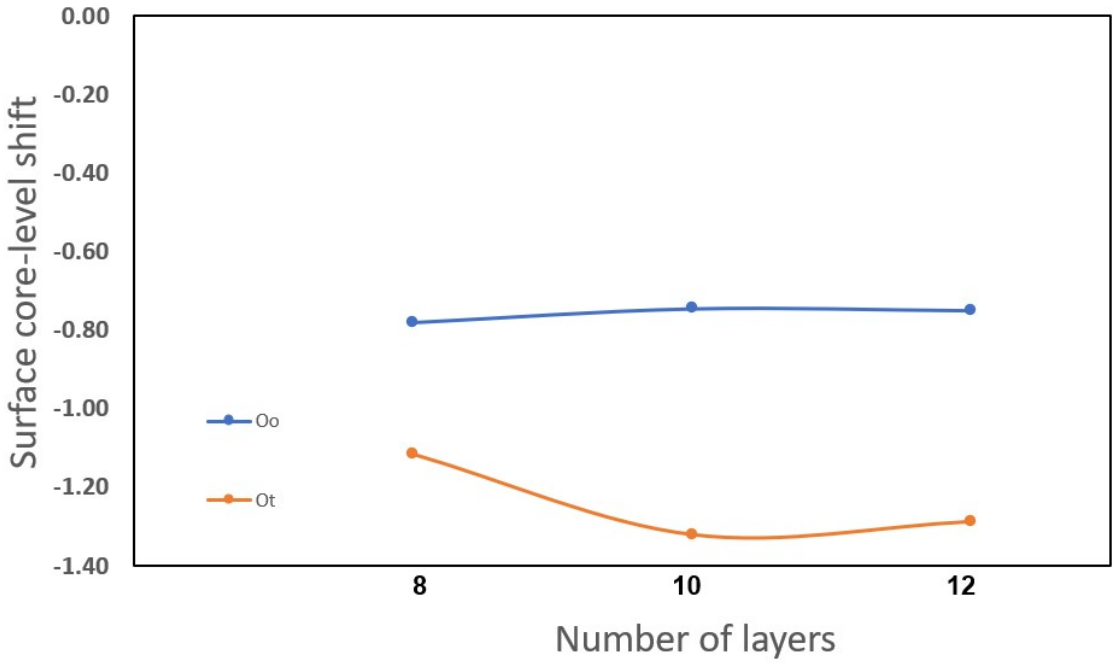

Figure S7. Convergence test showing the variation in calculated surface core level binding energy with the increasing slab thickness (number of layers) for surface oxygen on Co_3O_4 (100) surface, O_o represents the octahedrally coordinated surface oxygen and O_t represents the tetrahedrally coordinated surface oxygen.

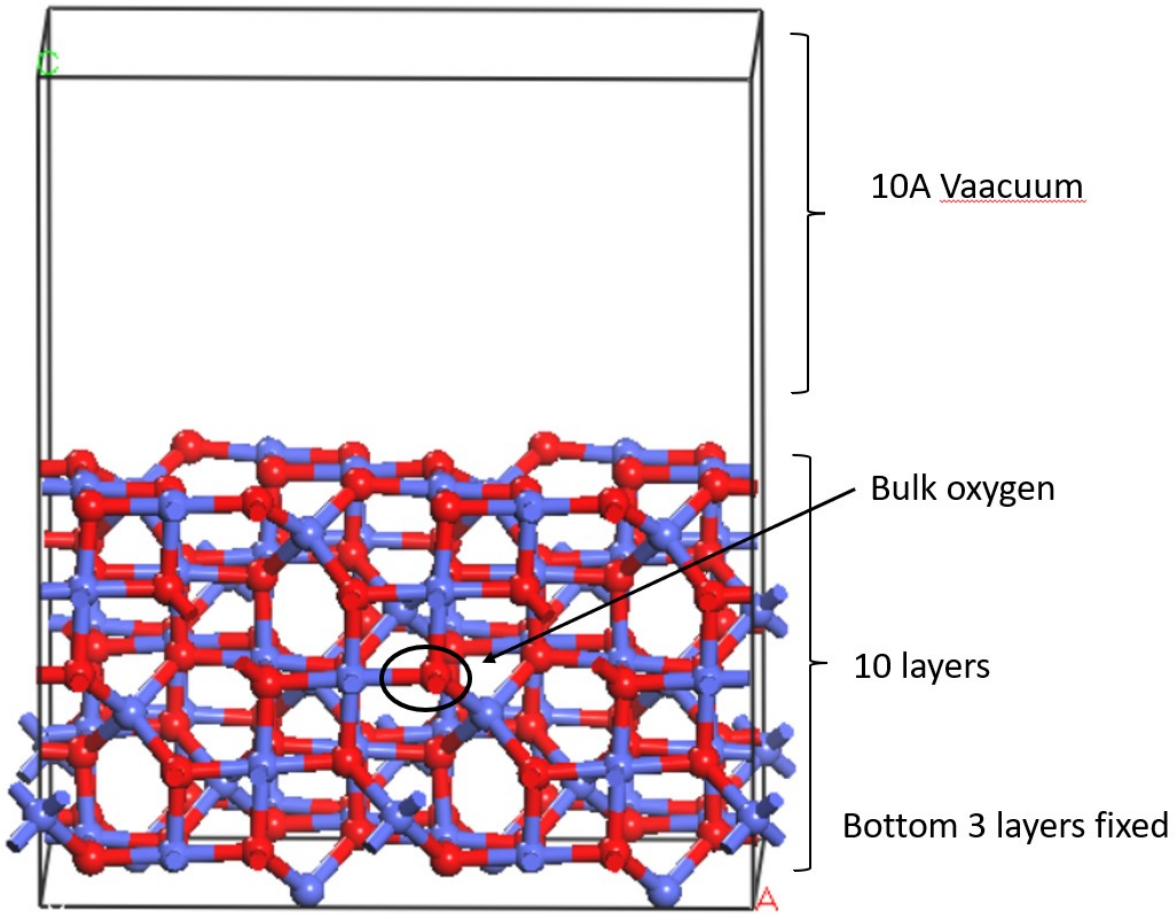

Figure S8. Representation of the system used to module Co_3O_4 (100) surface, slab size, illustrating the number of layers and vacuum thickness. The oxygen atom in the central layers representing the bulk oxygen is highlighted. Light blue and red balls represent Cobalt (Co) and oxygen (O) atoms, respectively.

The Rationale of Structure of Different Molecules Adsorbed on TMO surface

NiO has a typical rock-salt structure unit cell and NiO(100) terminal layer contains an equal number of nickel and oxygen atoms. All oxygen atoms on the clean surface layer are exactly the same; therefore any surface oxygen could be chosen for O1s core level binding energy calculation, to compare with the lattice oxygen O1s core level binding energy. Co_3O_4 unit cell has spinel structure, and the B-layer termination is more stable as discussed before, containing Co^{3+} and O. The oxygen atoms in Co_3O_4 are either connected to 2 Co^{3+} and 1 Co^{2+} or 3 Co^{3+}. Therefore, the O1s core level binding energy of surface oxygen needs to be calculated separately and compared to the bulk oxygen individually (all lattice oxygen atoms connected to 3 Co^{3+} and 1 Co^{2+}). The possible exposure of TMO samples to the atmosphere during the surface characterization process would allow the molecules in the atmosphere (most likely oxygen and carbon dioxide) to adsorb on the surface. These molecules might further react with each other to form various surface species, such as carbonates and bicarbonates. Moreover, it is also possible that the synthesized TMO surfaces are not perfectly stoichiometric and may contain possible surface vacancies. Thus, the probable adsorbates and their multiple adsorption configurations with clean or defective surfaces are considered and examined. When simulating various possible surface adsorbates on the TMO surface, we tested as many different configurations as possible and chose the most stable configuration for the core level binding energy calculation.

Adsorbates on Oxygen Vacancy surface

As discussed before, synthesized NiO materials might have intrinsic oxygen vacancy defects, especially under low oxygen concentrations, and Co_3O_4 is a reducible TMO which leads to easy formation of oxygen vacancy defects on its surface. Thus, the probable adsorbates and their adsorption configurations on clean and/or defective surfaces are considered and examined at the same time. We checked the relative stability of each configuration for every surface adsorbate, with possible vacancy site. We noticed that, for both TMO surfaces, when the oxygen species are interacting with the surface with oxygen defect sites, one of the oxygen atoms in the adsorbate would fill into the vacancy site to form the most stable adsorption configuration. For example, when O_2 molecule is adsorbed on the surface with oxygen vacancy defects, the most stable configuration would be the same as an O atom adsorbed on the clean perfect surface. Similarly, a hydroxyl group adsorbed on oxygen defective surface would be like a hydrogen atom adsorbed on clean surface; adsorbed CO_3 and HCO_3 on oxygen defective surface would be the same as adsorbed CO_2 and HCO_2 on clean surface, respectively.

The Choice of Oxygen

After the most stable configuration is obtained, we chose the oxygens in the adsorbed species or the surface oxygen which is directly affected by the surface adsorbates/vacancies to perform O1s core level binding energy calculations. The experimental XPS shifts could be referring to any possible oxygens on the sample surface. Hence, all potential oxygen candidates needed to be tested. For CO_2 adsorbed on NiO(100) surface (Figure S9a), using U values of 2eV and 5.3eV respectively, the calculated core level binding energy shifts difference between O2 and O2' is less than 0.05eV. Hence, it is believed that these two oxygen atoms have similar environment and only one of them need to be tested in the full range of DFT+U calculation. Similar situations were observed for CO_3 and HCO_3 adsorbed on NiO and Co_3O_4 surface (Figure S9b-e, g, h), the

calculated core level binding energy shifts for O1 and O1' in these cases are within the DFT accuracy (~0.1eV), despite the choice of U value. The only exception is that CO_2 on Co_3O_4 (100) surface (Figure S9f), as we could notice in the adsorption configuration, that O2 and O3 are slightly different on the surface. The calculated core level binding energy shifts using U value of 3.5eV is very similar (~1.3eV), yet when using U value of 6eV, the calculated shifts become 0.3eV and 0.7eV. Thus, both oxygen atoms are reported, and this further confirms that the choice of U value is very important for surface sensitive phenomena.

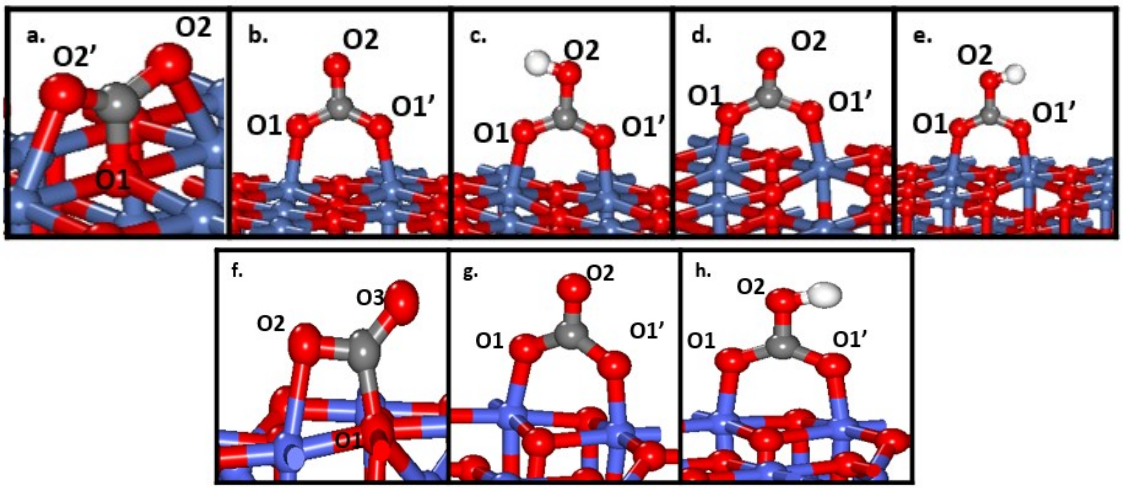

Figure S9. Structures of various surface adsorbates on NiO (100) surface evaluated to comparing with experimental XPS core level binding energy shifts. (a)adsCO_2 (b)adsCO_3, (c)adsHCO_3 and (d)adsCO_3 (e)adsHCO_3 near Ni vacancy site. Structure of various surface adsorbates on Co_3O_4 (100) surface evaluated to comparing with experimental XPS core level binding energy shifts. (f)adsCO_2 (g)adsCO_3 and (h)adsHCO_3.Dark blue, light blue, red, grey, and white balls represent nickel (Ni), cobalt (Co), oxygen (O), carbon (C) and hydrogen (H) atoms, respectively.

Adsorption energies of various adsorbates

Table S1. Calculated adsorbed energies of various adsorbates on NiO(100) surface using different U values

U value (eV)	1	2	3	4	5.3	6
NiO (100) surface						
$\frac{1}{2}H_2 + {}^* = {}^*H$	-0.44	-0.65	-0.87	-1.01	-1.21	-1.28
$\frac{1}{2}O_2 + {}^* = {}^*O$	-1.27	-1.35	-1.63	-1.74	-1.89	-2.01
$O_2 + {}^* = {}^*O_2$	-0.82	-1.12	-1.32	-1.54	-1.78	-1.91
$H_2O + {}^* = {}^*OH + \frac{1}{2}H_2$	-1.53	-1.39	-1.19	-1.02	-0.93	-0.78
$CO_2 + {}^* = {}^*CO_2$		-1.25	-1.39	-1.62	-1.89	-1.95
$\frac{1}{2}H_2 + CO_2 + {}^* = {}^*HCO_2$		-2.64			-3.22	
$\frac{1}{2}O_2 + CO_2 + {}^* = {}^*CO_3$		-2.65			-1.94	
$\frac{1}{2}H_2 + \frac{1}{2}O_2 + CO_2 + {}^* = {}^*HCO_3$		-2.74			-2.01	
NiO (100) surface with O vacancy		-1.02			-2.22	
$\frac{1}{2}H_2 + {}^* = {}^*H$		-0.69			-1.34	
$CO_2 + {}^* = {}^*CO_2$						
$\frac{1}{2}H_2 + CO_2 + {}^* = {}^*HCO_2$		-1.23			-1.98	
NiO (100) surface with Ni vacancy						
$\frac{1}{2}H_2 + {}^* = {}^*H$		-0.63			-1.28	
$\frac{1}{2}O_2 + {}^* = {}^*O$		-1.25			-1.74	
$O_2 + {}^* = {}^*O_2$		-1.05			-1.56	
$H_2O + {}^* = {}^*OH + \frac{1}{2}H_2$		-1.48			-1.07	
$CO_2 + {}^* = {}^*CO_2$		-1.73			-1.12	
$\frac{1}{2}H_2 + CO_2 + {}^* = {}^*HCO_2$	-2.32	-2.26	-2.52	-2.64	-2.86	-2.99
$\frac{1}{2}O_2 + CO_2 + {}^* = {}^*CO_3$		-1.97			-2.64	
$\frac{1}{2}H_2 + \frac{1}{2}O_2 + CO_2 + {}^* = {}^*HCO_3$		-2.58			-2.31	

Table S2. Calculated adsorbed energies of various adsorbates on Co_3O_4(100) surface using different U values

U value (eV)	1	2	3.5	5	6
Co_3O_4 (100) surface					
$\frac{1}{2}H_2 + {}^* = {}^*H$	-0.63	-0.82	-0.98	-1.21	-1.36
$\frac{1}{2}O_2 + {}^* = {}^*O$	-1.41	-1.02	-1.12	-0.94	-0.87
$O_2 + {}^* = {}^*O_2$	-0.98	-0.87	-0.69	-0.45	-0.24
$H_2O + {}^* = {}^*OH + \frac{1}{2}H_2$		-0.52	-0.89	-1.33	-1.86
$CO_2 + {}^* = {}^*CO_2$		-0.65	-0.74	-0.80	-0.78
$\frac{1}{2}H_2 + CO_2 + {}^* = {}^*HCO_2$	-1.18	-1.42	-1.94	-2.01	-2.23
$\frac{1}{2}O_2 + CO_2 + {}^* = {}^*CO_3$		-0.89	-0.96	-1.32	-1.45
$\frac{1}{2}H_2 + \frac{1}{2}O_2 + CO_2 + {}^* = {}^*HCO_3$	-2.41	-2.53	-2.23	-1.83	-1.64

Carbonaceous species, such as $*CO_2$, $*HCO_2$, $*CO_3$ and $*HCO_3$, can be formed during the exposure of transition metal oxide surface to the atmosphere. When CO_2 in the atmosphere is adsorbed, it is possible to interact with other surface adsorbed species, such as *OH, *H, $*H_2O$, to form various carbonate and bicarbonate species. The reaction mechanism of surface adsorbed carbonaceous species formation is beyond the scope of this study. The adsorption energies reported in Table S1 and S2 are based on the surface reaction reported in the table. However, the carbonaceous species could be formed via other reactions, for example, $CO_2 + H_2O = HCO_2 + OH$. Therefore, the adsorption energy could be calculated differently based on the possible surface reactions.

CO adsorption energy

CO adsorption energies on NiO (100) and Co_3O_4 (100) surfaces are calculated using different U values (as shown in the figures below). For NiO (100), the experimental CO adsorption energy is around -0.30eV (reported in multiple literatures, for example, Phys. Rev. Lett. 87, 086101, 2001 and Surface Science, Volume 325, Issue 3, L421-L427, 1995); for Co_3O_4, unfortunately, we couldn't find any reliable experimental data of CO adsorption energy on Co_3O_4 (100) surface. On both surfaces, the calculated CO adsorption energy depends on the U value and changes monotonically as the U value changes from 1-6eV, a trend very similar to what was observed for CuO (111) in the literature. However, since the PBE functional is known to over-predict CO adsorption energy, energies computed using PBE are lower than -0.3 eV for all U values. Hence, we also calculated the CO adsorption energy using the revPBE functional (which is considered more reliable for predicting CO adsorption energies) and we found out that the U value of 2eV, suggested as an appropriate U-value for NiO (100) based on XPS data, also predicted adsorption energy of CO to be -0.22eV, which is reasonably close to the experimental data.

This additional data on CO adsorption energies prediction further confirm that the surface U-value benchmarked using the XPS data also predicts adsorption and reaction energies correctly. The same conclusion was also drawn for CuO in our previous studies.

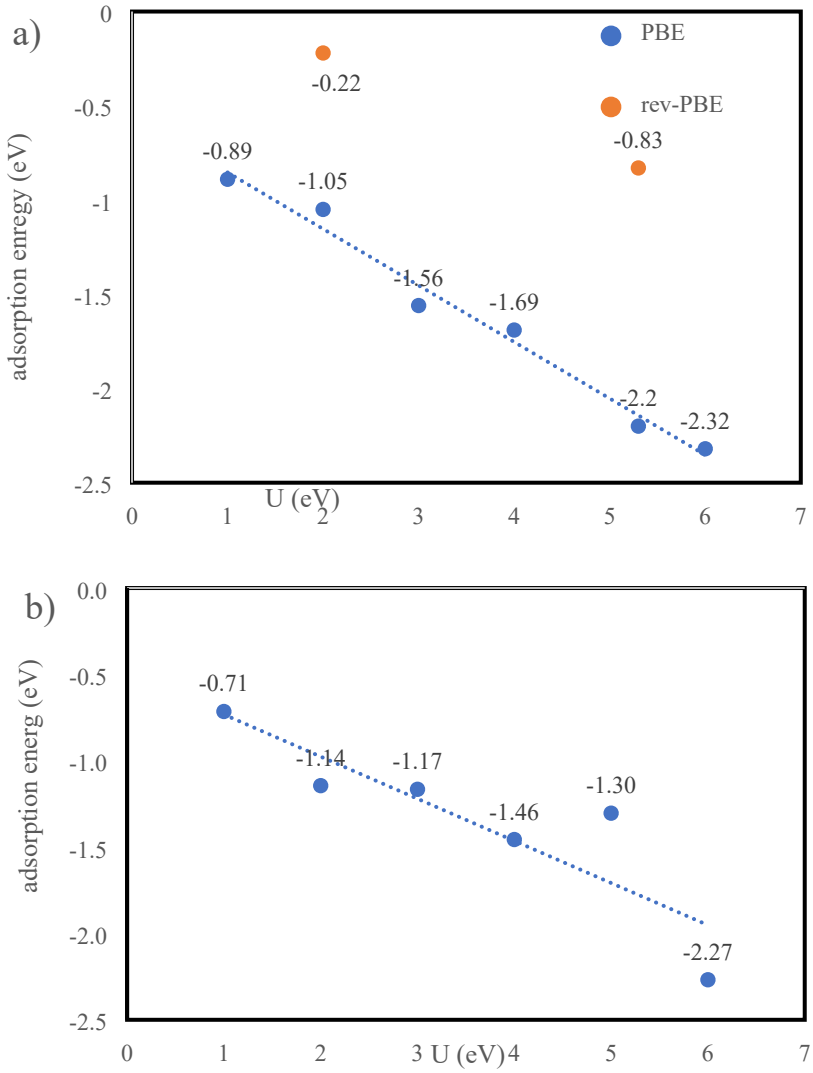

Figure S10. DFT-predicted CO adsorption energy on a) NiO (100) and b) Co_3O_4 (100) surface with different U values